A.

human iPSCs	♂	♀
Insulin Sensitive (I-Sen)	5	5
Insulin Resistant (I-Res)	5	5

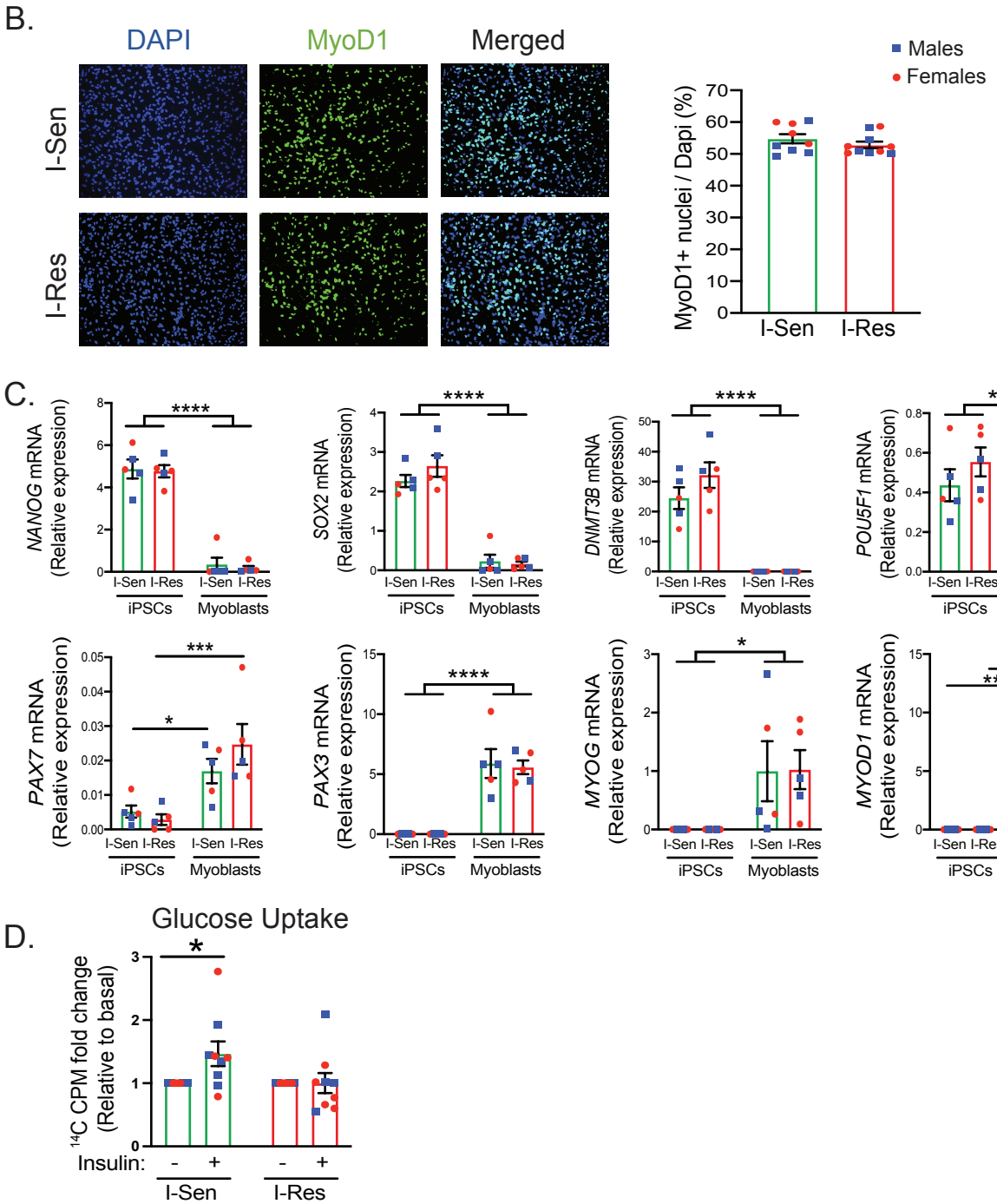

Suppl. Figure 1: I-Sen and I-Res iPSCs characterization and differentiation into myoblasts.
A) The cohort was composed of 10 insulin sensitive (I-Sen) and 10 insulin resistant (I-Res) subjects, 5 males and females each. I-Sen and I-Res iPSCs were differentiated into myoblasts (iMyos) as described in Methods. B) Representative MyoD1 immunostaining (green) in I-Sen and I-Res iMyos and quantification of MyoD1 positive regular growing cells expressed as a percentage relative to DAPI stain (n = 9 I-Sen, and n=10 I-Res). The data were subjected to unpaired t test (n.s. = non-significant). C) Gene expression of pluripotency markers and myogenic markers normalized to an internal control (TBP) in iPSCs and iPSC-derived myoblasts. Data are means ± SEM, n = 5/group. * P <0.05, ** P <0.01, *** P < 0.001, **** P < 0.0001 iPSCs vs myoblasts, one way ANOVA followed by correction for multiple comparison by controlling the FDR. D) 2-DOG glucose uptake data represented as relative to the basal state in iMyos stimulated with 100nM of insulin for 30 mins. Data are means ± SEM, n = 9/group, * P < 0.05 basal vs insulin, one sample t- test.

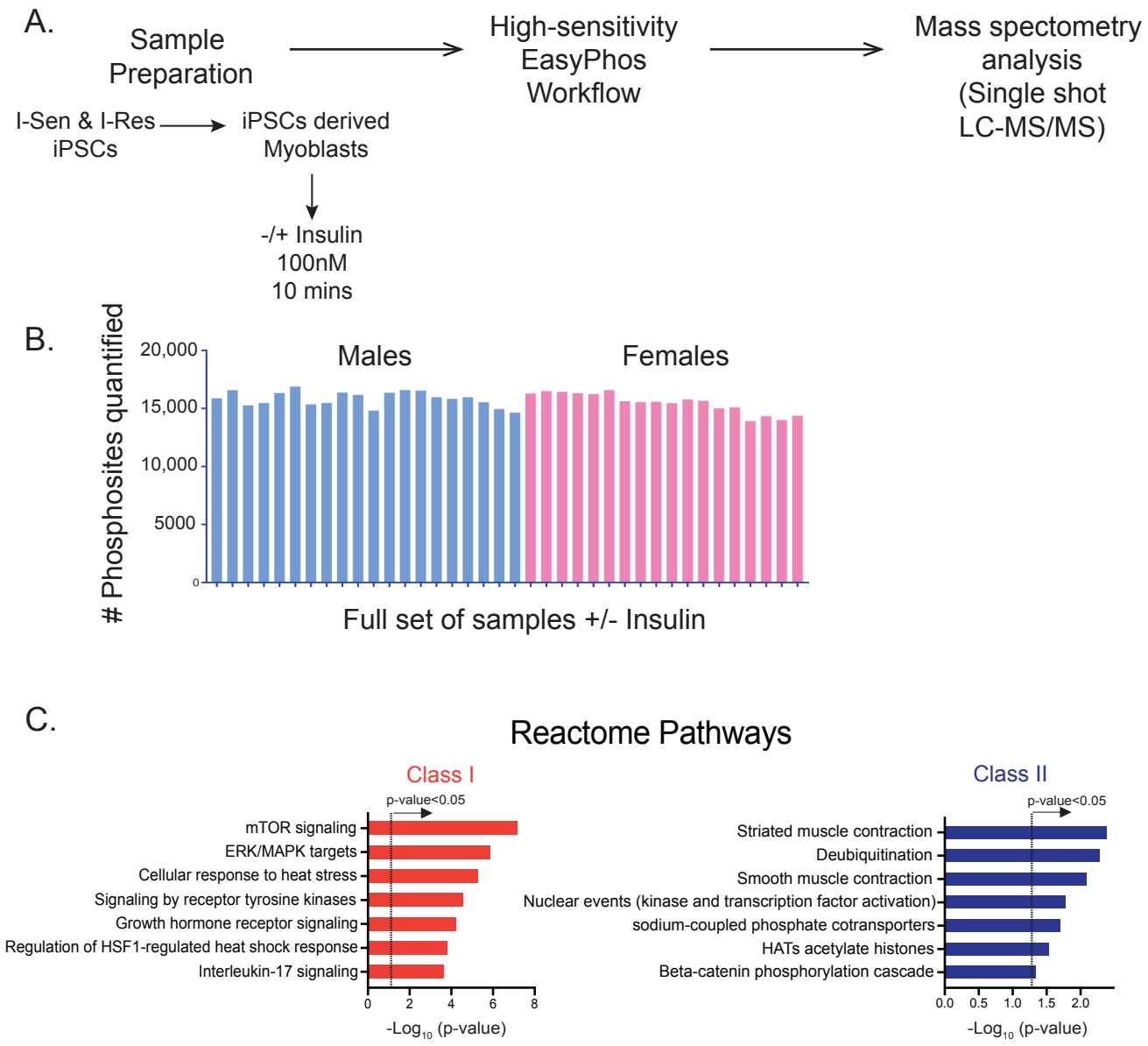

Suppl. Data Figure 2: Phosphoproteomics workflow and overview.
A) Phosphoproteomics workflow and experimental design. B) Quantification of the number of phosphosites in each of the cell lines +/- insulin. C) List of most enriched Reactome pathways representing phosphosites in Class I and Class II ($P < 0.05$). Plots are -Log10-transformation of p-values.

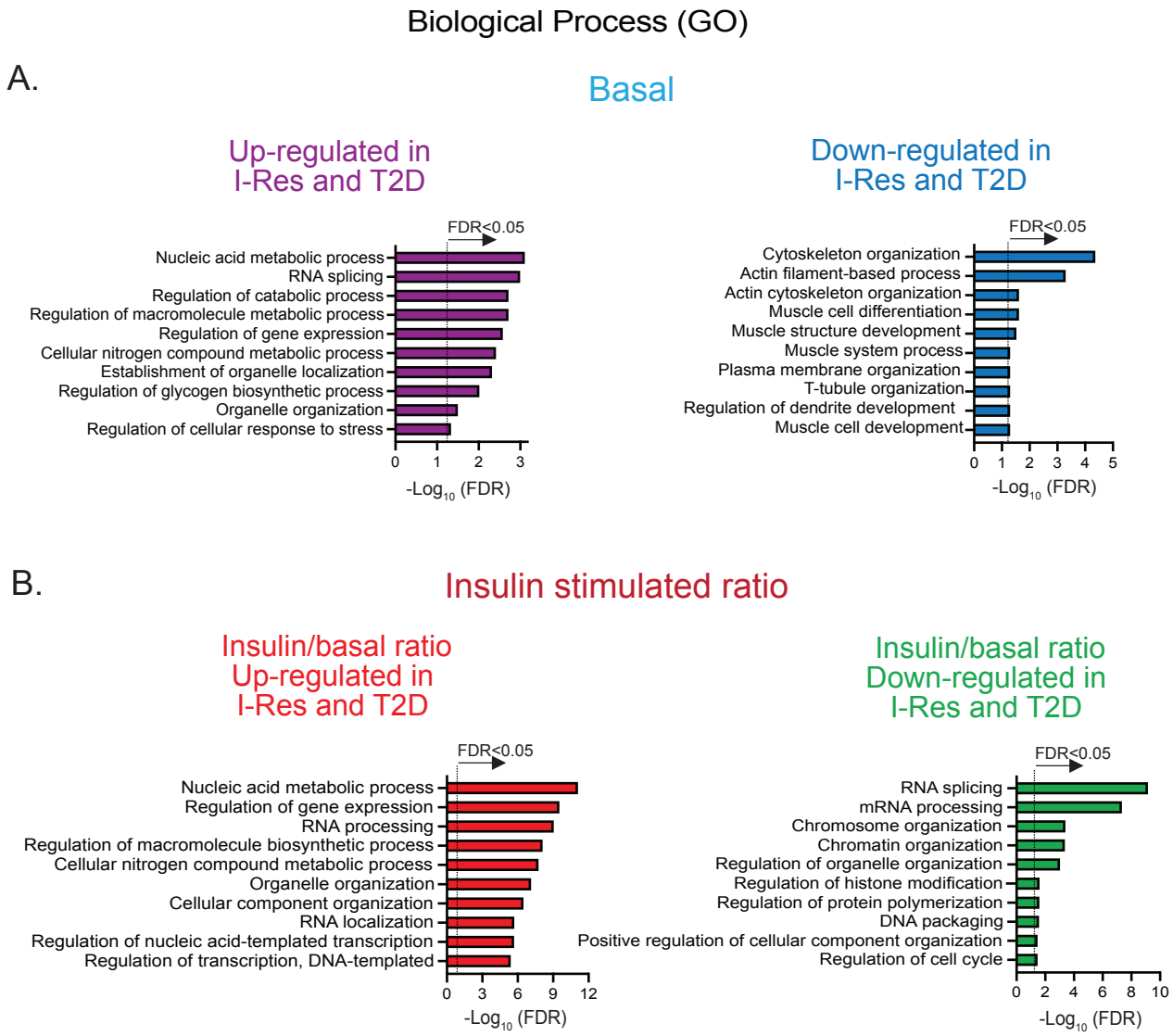

Suppl. Data Figure 3: Biological processes associated with insulin resistance in non-diabetics and T2D. A, B) GO biological processes showing the most significant enriched biological pathways altered in non-diabetics and T2D at the basal state and in the insulin stimulation ratio (FDR<0.05). The colors of the bar match the associated phosphosites changes in each of the pathways represented on the signaling map in figure 4.

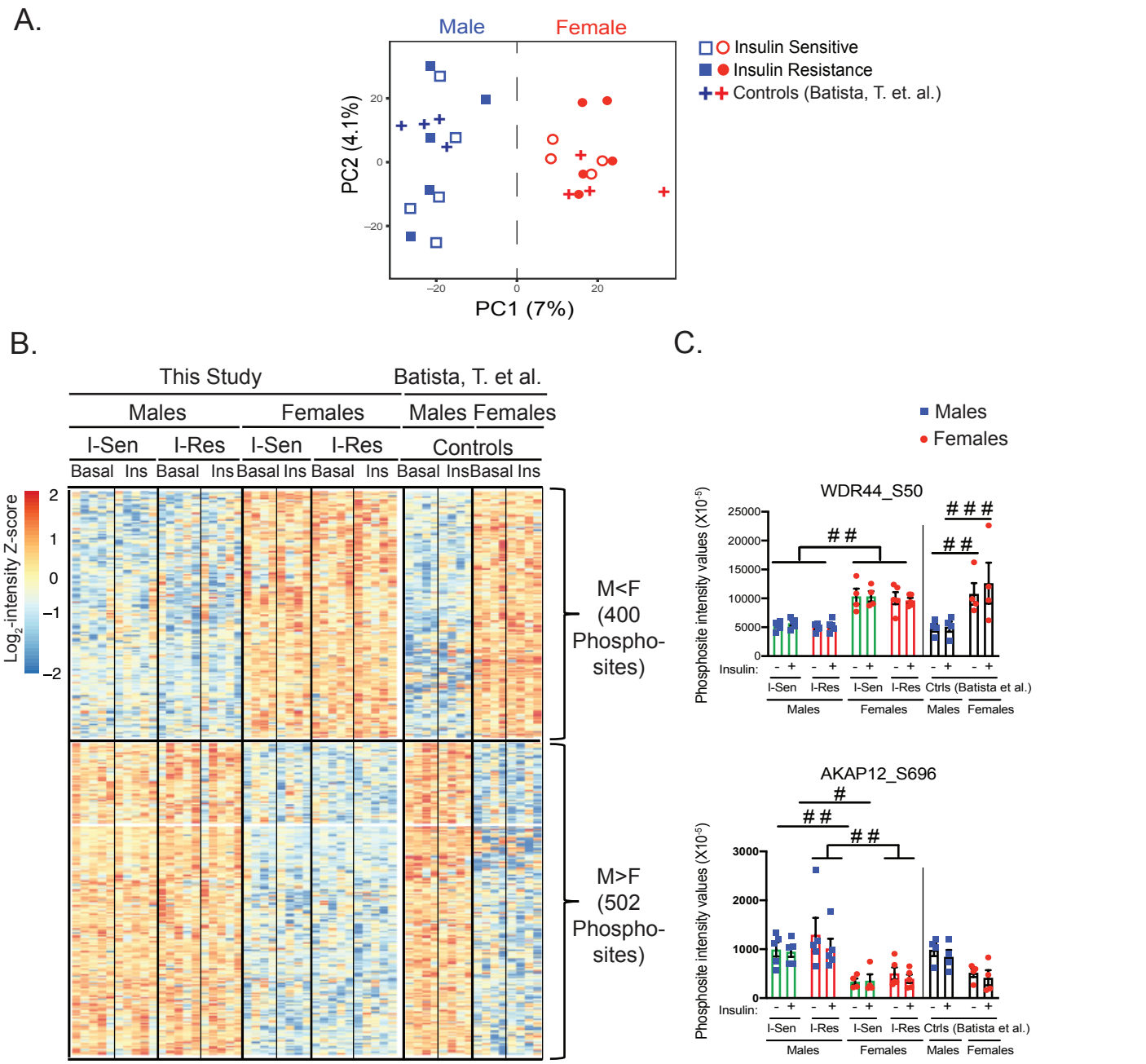

Suppl. Data Figure 4: Replication of protein phosphorylation changes underlying sexual dimorphism. A) PCA plot showing the separation of the phosphoproteome data by subject sex (blue: males, red: females) and insulin sensitivity status (open shape: insulin sensitive, filled shape: insulin resistant) between this study (circles and squares) and controls iMyos from (20) (plus sign) after surrogate variable analysis (SVA) adjustment. B) Hierarchical clustering of the peptides showing sexual dimorphism. Rows represent Z-scores of the log2-transformed intensity of phosphopeptides for each sample labeled in the column after SVA adjustment. C) Quantification of representative phosphosites. WD repeat-containing protein 44 (WDR44), A-kinase anchor protein 12 (AKAP12). Data are means ± SEM of phosphosite intensity values (x10-5). # P<0.05, # # P<0.01, # # # P < 0.001 males vs females, two-way ANOVA followed by correction for multiple comparison by controlling the FDR.

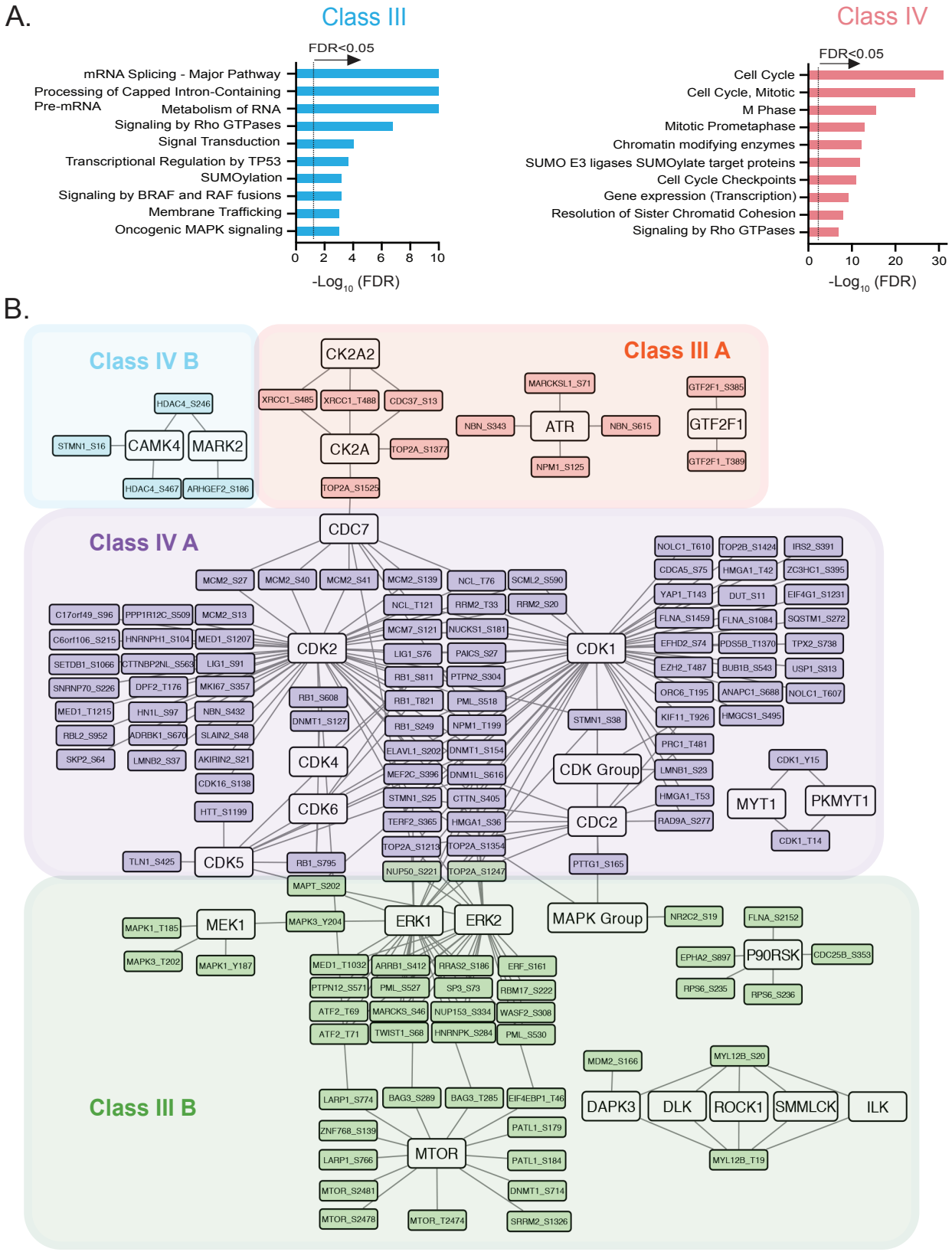

Suppl. Data Figure 5: Biological pathways and kinases modulating sexual dimorphism.
A) List of most enriched Reactome pathways representing phosphosites in Class III and Class IV. Plots are -Log10-transformation of FDR. B) Kinase-substrate map showing significantly enriched kinases and their predicted substrates for the class III and IV A-B sexually dimorphic phosphosites. The map is drawn using the Cytoscape software (3.8.0) and Adobe Illustrator 2020.